Assessing the effect of aromatic residues placement on α-helical peptide structure and nanofibril formation of 21-mer peptides

Journal:	*Molecular Systems Design & Engineering*
Manuscript ID	ME-ART-07-2019-000082.R2
Article Type:	Paper
Date Submitted by the Author:	01-Dec-2019
Complete List of Authors:	Solemanifar, Armin; University of Queensland, School of Chemical Engineering Nguyen, Tuan; University of Queensland, Environment Centres, Sustainable Minerals Institute Laycock, Bronwyn; University of Queensland, School of Chemical Engineering Shewan, Heather; University of Queensland, School of Chemical Engineering Donose, Bogdan; University of Queensland, School of Chemical Engineering Creasey, Rhiannon; University of Queensland, School of Chemical Engineering

Design System Application Statement:

This manuscript describes how the incorporation of aromatic residues into a de novo peptide designed for alpha-helical conformation affects the secondary structure. Here, we have used as a base model a peptide sequence that forms a stable coiled-coil α-helical fibril and modified the sequence by substituting aliphatic residues with aromatic residues (phenylalanine and/or tryptophan) using different combinations and positions. Our experimental and molecular dynamics simulation work suggests that tryptophan residues disrupt the α-helical structure, while incorporating phenylalanine residues at certain positions in the peptide sequence has less overall impact. Our manuscript adds to the body of knowledge of design constraints for α-helical peptide structures that include aromatic amino acids, which is important given the functionality that aromatic can introduce to peptide structure. This work will be beneficial to those authors wanting to incorporate aromatic residues into coiled-coil α-helical peptides without compromising the stability of the α-helical structure.

Table of contents entry:

Aromatic residues were used to replace the aliphatic residues of an α-helical peptide to investigate changes on the peptide structure.

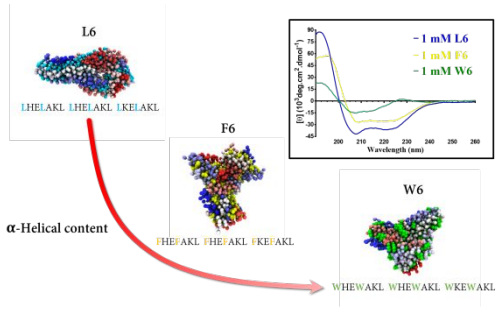

ARTICLE

Assessing the effect of aromatic residues placement on α-helical peptide structure and nanofibril formation of 21-mer peptides

Received 00th January 20xx,
Accepted 00th January 20xx

DOI: 10.1039/x0xx00000x

Armin Solemanifar,[a†] Tuan A. H. Nguyen,[b] Bronwyn Laycock,[a] Heather M. Shewan,[a] Bogdan C. Donose,[a] and Rhiannon C. G. Creasey [a†]

Coiled-coils with defined assembly properties are attractive materials for the manufacture of peptide-based hybrid nanomaterials. In tailoring such peptide assemblies, the incorporation of aromatic residues is increasingly being investigated due to their potential to deliver controllable functionalities, such as interaction with aromatic porphyrins, carbon nanotubes, or graphene. Aromatic residues have the potential to either destabilise or stabilise the α-helical peptide structure, depending on the quantity, type, combination, and position of these residues in the peptide chain. In this work, we used a known synthetic three heptad repeat peptide containing no aromatic residues as an α-helical template. We then substituted the aliphatic residues with two different types of aromatic residues (phenylalanine and tryptophan), varying their number, position, and combination in the peptide chain as a preliminary assessment of the impact on peptide architecture. Circular dichroism (CD) spectroscopy combined with coarse-grained (CG) and all-atom (AA) molecular dynamics (MD) simulation were used to analyse the peptide structure and assembly. Aromatic residues designed to be within the hydrophobic core were had impact on self-assembly than those placed on the outer face of the coil. Tryptophan was seen to destabilise α-helical structure more than phenylalanine, potentially due to steric hindrance and hydrogen-bonding interactions. Using atomic force microscopy (AFM) and supported by CG-MD simulation, substituting all phenylalanine residues with tryptophan appeared to completely destabilise fibril-formation propensity. Subsituting tryptophan into the first heptad repeat was seen to have a greater impact on fibril formation compared to subtitution into the third heptad repeat, suggesting the importance of sequence design. These results add to the body of knowledge used to inform the design of α-helical peptides when incorporating aromatic residues.

Introduction

The α-helical structure of peptides is one of the most abundant and stable ordered secondary structures among proteins.[1] Peptides based on these proteins are attractive building blocks for self-assembly in biological applications, with well-defined folded and compact structures. Additionally, they can be tailored to deliver desired functionalities via their chemical side groups. Higher-order conformations can be designed into such peptides by utilising self-assembly via non-covalent interactions, such as hydrogen bonding, electrostatics, hydrophobic, and π-π interactions.[2] One of the known assembled structures of α-helices is the rope-like coiled-coil. Not only are coiled-coils (and α-helices) important in biology, but they may be exploited for applications in biomedical and materials science.[3-5] α-Helical coiled-coil peptides typically display a periodicity of 7 residues, with the positions labelled "*a*" through "*g*", consecutively.[6, 7] The helical stability of such peptides and their self-assembly depends on the type of residues present in these positions as well as their order.[8-10] In a coiled-coil structure, positions *a* and *d* are conventionally occupied by hydrophobic residues, forming a hydrophobic core.[11] Along with aliphatic residues, these positions may also be filled with hydrophobic aromatic residues such as phenylalanine (Phe), tryptophan (Trp), and tyrosine (Tyr).[12-14] The incorporation of such aromatic residues can be exploited in bioenergy,[15] biomedical and bionanotechnology applications, for example, via interaction with porphyrins,[16] carbon nanotubes[17, 18] or graphene.[19] Also, the role of aromatic residues in conferring electrical conductivity and their potential for electron transfer in peptides, proteins, and bacteria has been investigated.[20-22] Thus, understanding the design rules for peptides containing aromatic residues is timely and important.

Aromatic residues are known to promote self-assembly, particularly in β-sheet structures.[23-30] Less intensely studied is the incorporation of aromatic residues in the hydrophobic core of α-helical peptide structures.[31-34] Aromatic residues promote hydrophobic and π-π interactions and, in some cases, provide hydrogen bonding sites for intra- and inter-molecular stability. In addition, cation–π interactions between aromatic amino acids and the positively charged residues lysine and arginine

[a.] *The University of Queensland, School of Chemical Engineering, Brisbane, QLD 4072, Australia.*
[b.] *The University of Queensland, Environment Centres, Sustainable Minerals Institute, Brisbane, QLD 4072, Australia.*
† *Corresponding authors: a.solemanifar@uq.edu.au; and Rhiannon.creasey@gmail.com*

Electronic Supplementary Information (ESI) available: [Characterisation of peptide self-assembly and secondary structure using experimental, online tool, and molecular dynamics simulation]. See DOI: 10.1039/x0xx00000x

have been proposed to play an important role in stabilizing protein structure.[35] On the other hand, they have low helix forming propensity,[36] due primarily to their conformational rigidity and steric hindrance. These features may affect the self-assembly of coiled-coil α-helical structures depending on the sequence position, density, chemical properties, and combinations thereof.

By considering the above parameters, this preliminary study investigates the incorporation of either or both of two natural aromatic residues, Phe and Trp, into a typical fibril-forming α-helical sequence. These amino acids were chosen because of their potential for electron transport applications.[20, 37-39] The number and position (and combinations thereof) of these residues in the 21-mer peptide were varied. It should be noted that there are various possibilities for replacing the aliphatic residues at *a* and *d* positions in L6 with Phe and Trp; however, only five aromatic containing peptides were designed, and four were experimentally tested due to the interest in their electrical properties. The electrical properties of aromatic-containing peptides depend on the type and number of them incorporated and their spacing between each other.[20] Therefore, in a peptide containing aromatic residues, the secondary structure and peptide assembled form could play an important role in the peptide electrical properties and their potential application. The designs used herein were based on a known de-novo designed 21-mer peptide (L6)[22] that contains no aromatic residues (Table 1).

To design peptides that self-assemble into coiled-coiled α-helical structures, we considered several parameters. One of the main driving forces for self-assembly of α-helices into coiled-coil structures is hydrophobic interactions between the α-helices (in terms of stabilisation).[40] Positions *a* and *d* in the α-helices are conventionally occupied by hydrophobic residues such as leucine (Leu), isoleucine (Ile), valine (Val), or alanine (Ala) to make a hydrophobic core that is compatible with a coiled-coil formation.[11] Therefore, we used an aliphatic hydrophobic residue, Leu, in the *a* and *d* positions in L6. Additionally, in coiled-coil design peptides, positions *e* and *g* are usually occupied by ionisable amino acid residues with other polar residues often occupying positions *b*, *f*, and *e* to make a hydrophilic surface.[41-43] However, expanding the hydrophobic core to cover the *e* and *g* positions can increase the oligomerisation state of the coiled-coils due to the larger hydrophobic face for association.[44-46] While designing an α-helical structure, it is important to consider the use of amino acid residues with relevantly high α-helix forming propensity. Ala and Leu are considered to be among the most helix favouring natural amino acids.[10] As a result, we decided to expand the hydrophobic core and include Ala and Leu as hydrophobic residues in positions *e* and *g*, respectively. Another parameter that affects the coiled-coil α-helical peptide stability is its constituent length. By increasing the heptad repeat, the proportion of less stabilised amino acid residues decreases and stabilised interactions increase.[47, 48] The general designed α-helix coiled-coil peptides have three to six heptads (21 to 42 amino acid residues).[42] We focused our study by using three heptad repeats for the peptide length (maintaining the length at 21 amino acids). In future studies, we are keen to explore varying numbers of heptad repeats. After a peptide self-assembles into an α-helical structure, a higher order of structural changes, such as coiled-coil fibril formation, may be observed. There are different strategies in α-helical peptide sequence design to promote the formation of extended fibrils. A common design tactic uses the forced offsetting of α-helical monomers, for example, via the asymmetric inclusion of hydrogen bonding interactions in the hydrophobic core of the coiled-coil along with distribution of asymmetric charge residues.[49-52] Another strategy, which lacks explicit offset designs, is to drive fibril formation by "slippage" of vertically aligned residues in the same structural class (cationic, anionic, or hydrophobic), in which residues are located in same positions in the heptad.[11, 53-55] While this strategy has previously employed using exact heptad repeats,[55] several studies have demonstrated the extended fibril formation of inexact repeats based on this strategy.[11, 53, 54] Inspired by previously reported designs of this structural class,[11, 56] we designed a fibril forming α-helical L6[22] peptide with inexact heptad repeats where cationic residues (lysine and histidine) were aligned in position *b* and *f*, all glutamates were in position *c*, and hydrophobic residues (Ala and Leu) occupied positions *a*, *d*, *e*, and *g* (Table 1).

Table 1. Amino acid sequence of de novo designed peptides, including acetyl and amide capping. Sequences are denoted using an *a*-register. Phe and Trp residues are coloured yellow and green, respectively.

Peptide label	Sequence				
L6	Ac -	LHELAKL	LHELAKL	LKELAKL	- NH_2
Register		*a b c d e f g*	*a b c d e f g*	*a b c d e f g*	
F6	Ac -	FHEFAKL	FHEFAKL	FKEFAKL	- NH_2
Register		*a b c d e f g*	*a b c d e f g*	*a b c d e f g*	
W6	Ac -	WHEWAKL	WHEWAKL	WKEWAKL	- NH_2
Register		*a b c d e f g*	*a b c d e f g*	*a b c d e f g*	
F4W2	Ac -	FHEFAKL	FHEFAKL	WKEWAKL	- NH_2
Register		*a b c d e f g*	*a b c d e f g*	*a b c d e f g*	
W2F4	Ac -	WHEWAKL	FHEFAKL	FKEFAKL	- NH_2
Register		*a b c d e f g*	*a b c d e f g*	*a b c d e f g*	
F4	Ac -	LHEFAKL	LHEFAKF	LKEFAKL	- NH_2
Register		*a b c d e f g*	*a b c d e f g*	*a b c d e f g*	

Following these design rules, L6 adopts a stable α-helical structure that self-assembles into long and uniform fibrils at neutral pH.[22] L6 was designed to form fibrils through helical slippage of vertical alignment of amino acid residues in the same structural class as reported previously in other coiled-coil α-helical peptides with high thermostability.[11, 22, 56]

To replace aliphatic residues in L6 with aromatic residues in the first aromatic-containing peptide design, denoted F6,[22] six Phe residues replaced the aliphatic residues at the *a* and *d* positions. Then, all Phe residues were replaced by a bulkier aromatic residue (Trp) in the W6 design to investigate the use of a bulkier aromatic residue with greater electron transport capacity. While there are different ways to replace aliphatic residues in L6 with a combination of Phe and Trp, we designed a peptide,

denoted F4W2, that utilises a combination of four Phe and two Trp residues. In the F4W2 design, Trp residues in W6 at the first two heptad repeats were replaced by Phe residues to assess the effect of both types of aromatic residues. The W2F4 was designed (and modelled but not experimentally tested), with the Trp residues in the third heptad repeat of F4W2 replaced by Phe residues in the first heptad repeat. Finally, in the F4 design, tailored to have a reduced number of aromatic residues, three aromatic residues replaced the Leu residues in L6 at the *a* and *d* positions and also at the *g* position (on the outer face of the coiled-coil). Out of five designed peptides, only F4 had a Phe residue at the *g* position as an exploratory exercise. This design was chosen as the addition of an outer face aromatic residue was expected to introduce aromatic-aromatic interactions with the residues of other peptide monomers, making an interesting case for assessing the peptide secondary and self-assembly changes under these conditions. These 21-mer peptide sequences are shown in Table 1, with an acetylated N-terminus and amidated C-terminus. Both experimental work and simulations were used to characterise each peptide model. The secondary structure of the peptides was investigated using circular dichroism (CD) spectroscopy and analysed by BeStSel.[57, 58] In parallel, all-atom models and coarse-grained (CG) from molecular dynamics (MD) simulations were performed. Simulations of all-atom models on single peptide monomers were carried out for up to 1.2 μs to study possible peptide structures at local minimum energy levels as representative models of peptides at the lowest concentration where inter-molecular interactions are of importance. CG models (with MARTINI force field)[59-62] of each peptide were carried out up to 25 μs (100 μs in effective simulation time), revealing assembled structures such as fibrils where inter-molecular interactions are of importance.

The incorporation of aromatic residues resulted in a reduced α-helical content compared to the (aliphatic-only) negative control in all cases tested. Differences in the extent of disruption were associated with (most significantly) the type and location of these residues. This study adds to the knowledge of design constraints for α-helical peptide structures that include aromatic amino acids and is beneficial for designing α-helical peptides with interest in their electrical properties.

Experimental

Peptide preparation

Peptide L6 (Ac-LHELAKL LHELAKL LKELAKL -$CONH_2$, MW 2465.04 g/mol) was synthesised and purified by Genscript.[22] Peptides F6 (Ac-FHEFAKL FHEFAKL FKEFAKL -$CONH_2$, MW 2669.14 g/mol),[22] W6 (Ac-WHEWAKL WHEWAKL WKEWAKL-$CONH_2$, MW 2903.39 g/mol), F4W2 (Ac-FHEFAKL WHEWAKL FKEFAKL -$CONH_2$, MW 2747.25 g/mol), and F4 (Ac-LHEFAKL LHEFAKF LKEFAKL-$CONH_2$, MW 2601.13 g/mol) were synthesised and purified by Mimotopes (Australia) using FMOC chemistry. The final purity for all peptides was >95% as measured by HPLC (details in Appendix section in the supplementary document). The peptide content of the solid was determined by high sensitivity amino acid analysis for precise concentration calculations (Australian Proteome Analysis Facility, Sydney).

Peptide stocks were prepared from lyophilised powder in water (Ultrapure MilliQ, 18.2 MΩ) at a concentration of 10 mM and further diluted in water. For titration with sodium bicarbonate, 100 μM of 10 mM peptide at room temperature were mixed with 100 μM of sodium bicarbonate with desired concentration (calculated to reach pH 7.4).

MD simulations

All-atom MD simulation was conducted to assess secondary structures of all peptide sequences. The initial structure of all peptides were built in the right-hand α-helix conformation using PyMol[63] and were capped on the N-terminus and C-terminus by an acetyl group and an amide group ($CONH_2$), respectively. Using GROMACS 5.1 version [64] and CHARMM36 force field [65], one 21-mer peptide was immersed in TIP3P water model [66] with 1.5 nm solute-box boundary, forming a periodic simulation box of 5×5×5 nm^3. Counter ions were added to neutralise the charges of the peptide and salt concentration (NaCl) was set to 50 mM. The bond lengths between heavy atoms and hydrogen bonds were constrained using the LINCS [67] algorithm, while electrostatic interactions were treated by using the Particle-Mesh-Ewald [68] method with coulomb distance cut-off of 1 nm. Energy minimisation was conducted using the steepest descent algorithm by maximum 10,000 steps (1 nm energy step size) and stopped if the energy minimisation force became lower than 500 (kJ/mol.nm). The simulation was continued with an NPT ensemble at 298 K and 1 bar pressure, where the Verlet leap-frog integrator algorithm was used to propagate the dynamics of the system at 2 fs time steps. Based on Maxwell distribution, initial velocity was generated and recorded along with coordinates every 2 ps while energies were recorded every 5 ps. The system was simulated up to 1.2 μs. To analyse the data collected from all-atom MD simulation, the first 200 ns of simulation was omitted to reduce the bias of the initial representative structure. The root mean square fluctuation (RMSF) was calculated for C_α of each residue against its average position using the trajectory that contained the whole simulation time (peptide monomer was fixed [69] in the centre of simulation box in the trajectory prior to RMSF calculation).

The last frame of the simulation does not necessarily mean it shows the most stable and representative structure of the peptide. The free energy landscape (FEL) was determined to find a representative structure of the peptide. The FEL is usually presented in two variables: the radius of gyration (Rg) that reflects specific properties of the protein, and the root mean square deviation (RMSD). FEL figures were created using Mathematica software.[70] Representative structures of each peptide at their lowest Gibbs free energy were visualised using the VMD tool.[71]

CG MD simulations with Martini force field[59-62] were used to understand the peptide assembly better. An initial all-atom structure made by PyMol[63] was used to create CG Martini topologies of each peptide by using the martinize.py[59-62] script. The CG simulation box contained 28× 21-mer peptide monomers randomly distributed in a cubic box (12×12×12 nm^3).

The CG simulation was repeated 3 times for each peptide sequence using a random seed when generating the simulation box of peptide monomers. CG MD simulations were conducted in an NPT ensemble with temperature and pressure kept at 303 K and 1 bar, respectively. The simulations were carried out for up to 25 μs, which is equivalent to 100 μs effective simulation time. It is worth noting that the Martini force field uses a 4:1 atom/CG-bead mapping to represent peptide backbone and side chains and a 3:1 atom/CG-bead mapping for the aromatic ring of PHE. Therefore, the dynamics observed compared to atomistic models are faster.[72] To adjust for this, we chose a scale factor of 4 that has been used as a standard conversion factor [59, 72, 73] to scale the time axis when interpreting simulation results with CG model.

CD spectroscopy

Peptide samples were prepared in water (Ultrapure MilliQ, 18.2 MΩ). CD spectra were collected using a JASCO-815 spectrometer at 25°C between 260 and 190 nm wavelength and averaged over 10 scans. The CD sensitivity was set to standard and spectra were scanned continuously at 50 nm/min speed with 1 nm bandwidth, 0.1 nm data integral, and 4 s integration time.

CD spectra analysis with BeStSel

The BeStSel method[57] was used for analysing CD spectra. Mean residue ellipticity values were divided by 1000 and submitted, along with the wavelength for each value, into the website.[74] The "mean residue ellipticity/1000" was chosen as an input unit, and the scaling factor was chosen to be 1 for all measurements.

AFM sample preparation and imaging

Silicon wafers (coated with a naturally grown silica layer of 2-4 nm) were diced (5×5 mm), washed in 10% H_2SO_4, rinsed in ethanol and deionised (DI) water and then cleaned (30 minutes) using a UV/Ozone unit (BioForce). 20 μL of peptide suspension (1 mM peptide along with the required sodium bicarbonate concentration to reach pH 7.4) was deposited onto the clean wafers and left for 2 hours for incubation (inside a closed petri dish with wet Kimwipes™ inside the petri dish to maintain humidity). Then, the excess liquid was removed, and the wafers left to dry for 24 h under ambient conditions in covered containers.

Images were acquired using a Cypher AFM (Oxford Instruments) operated in air (AC mode). HA NC Etalon (NT-MDT Spectrum Instruments) probes of less than 10nm contact radius were used to obtain 256x256 pixel images at 1Hz.

Figure 1 (a) and (e) were prepared as per reference.[22] Briefly, AFM micrographs were collected using an Asylum MFP3D SPM (Oxford Instruments) using Etalon HA NC probes (AC mode) under ambient conditions. Peptides were prepared as above on OTS-coated silicon wafer.

Image analysis was undertaken using freeware Gwyddion (http://gwyddion.net) v2.54.

Rheology

A Haake Mars 3 (Thermo Scientific) stress-controlled rotational rheometer with Peltier controlled element set to 25 °C, with 35 mm titanium plates, was used for rheological measurements to determine the physical properties including viscous and elastic behaviour of the peptide samples at 5 mM concentration after mixing with sodium bicarbonate. Parallel plates were chosen and operated at a gap of 500 to 800 μm due to the small sample volumes available. Prior to measurement, the gap error was zeroed at 4 N and gap error calculated as previously described.[75-77] Samples F4, F6, W6, and F4W2 were titrated by the required sodium bicarbonate with minimum one hour wait period allowed to reach pH 7.4 (where pH rose by the loss of CO_2 from the sodium bicarbonate in the sample) prior to placing on the rheometer plate surface, as the loss of CO_2 was inhibited in the 0.5 mm gap between plates. These four samples were able to flow, and preshear history had little influence on sample rheology. Upon titration with sodium bicarbonate, L6 formed a gel-like solid in less than 3 minutes that could not be transferred to the plate surface without breaking. For L6, titration with sodium bicarbonate and gelation were carried out on the bottom plate of the rheometer with the top plate carefully positioned 1.5 hours after the start of titration to fill the plate gap while avoiding fracture of the formed gel. Roughened (sandblasted) plates were used to prevent slip during measurement. Storage (G') and loss (G") modulus were measured in the linear viscoelastic regime (LVR) at a stress of 0.1 Pa (for L6, F6, F4, and F4W2) or 0.05 Pa (for W6) using a frequency sweep between 0.6 and 60 rad/s. The LVR was determined using an amplitude sweep at three frequencies within the desired frequency range. A shear stress sweep was carried out from 0.1 to 1000 Pa to measure viscosity. Viscosity was calculated as a function of torque and rotation rate by fitting a power-law equation to each section of the curve as described by Davies and Stokes.[76]

Results and Discussion

As previously reported,[22] L6 formed self-assembled fibrils at physiological pH (pH=7.4), which was achieved by slow titration in sodium bicarbonate at room temperature.[22] AFM imaging[22] showed L6 assembling into fibrillar structures, and CG Martini modelling also resulted in largely one-dimensional forms (Figure 1). Moments of inertia (MOI) were calculated to obtain more insights into the structure and shape of the assembled peptide structure. Changes in geometry of the assembled peptides could be quantified by calculating the MOI of the largest cluster aligned to the principal axes (I_X, I_Y, I_Z). Then, to assess the one-dimensionality of the cluster, aspect ratios of the MOIs ($MOI_{(Z/X)}$) were calculated. For spherical objects, values of I_x, I_y , and I_z are similar while for rod-shaped objects, MOIs along two principal axes have similar values but are larger than the MOI along third principal axes (e.g. $I_X \approx I_Z > I_Y$).[78] The calculated $MOI_{(z/x)}$ for L6 was found to be 6.39 (Figure 1 and Table S1).

The measurement of G', G" as a function of frequency (Figure 2a) and viscosity as a function of shear stress (Figure 2b) allows us to describe each of these peptide samples as demonstrating viscous, viscoelastic liquid or gel-like behaviour. Sample L6 is the only one to demonstrate gel formation, where G' is greater than G" (Figure 2a). We hypothesise that upon the formation of

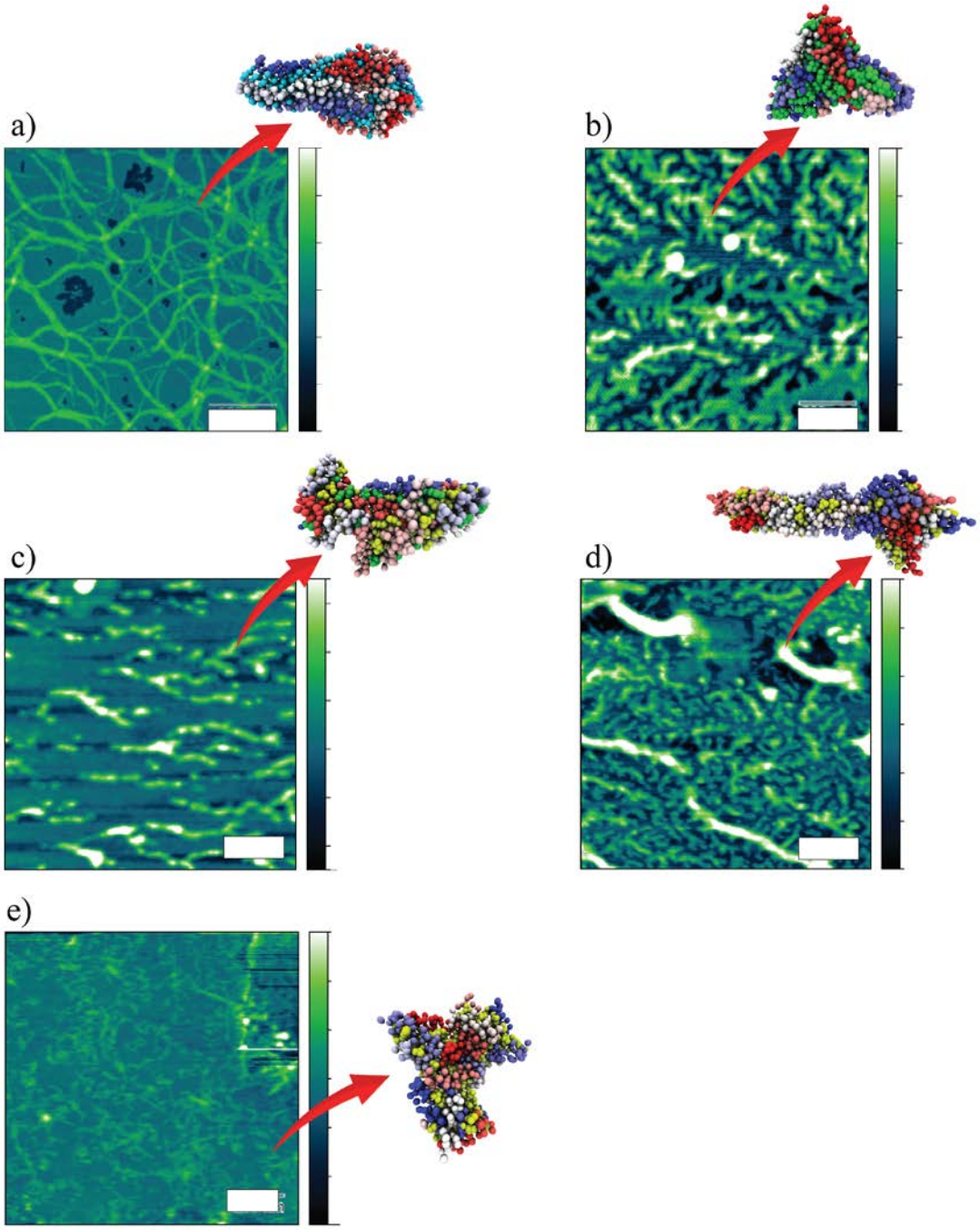

Figure 1. AFM height images of for (a) L6, (b) W6, (c) F4W2, (d) F4, and (e) F6 peptides with lateral scale bars 200 nm and z-colour scale bars 12 nm. The largest CG clusters for (a) L6, (b) W6, (c) F4W2, (d) F4, and (e) F6 at 25 μs are located at top right of their AFM images with Phe and Trp residues coloured yellow and green, respectively, and different peptide chains are presented in different colours.

fibrils by the slippage mechanism (initiated by α-helical peptides forming coiled-coils), the fibril-fibril association leads to the formation of physical cross-linking (gel formation) that is triggered by the net molecular charge as a result of pH change. We suggest that this behaviour agrees with the network structure observed from the AFM images shown in Figure 1 and transmission electron microscopy (TEM) images included in Figure S1. Viscosity was not measurable as the weak gel did not flow under shear but demonstrated brittle fracture.

The secondary structure of peptides may be determined using CD spectroscopy. Typical α-helical features (a maximum at 190 nm and minima at 208 nm and 222 nm)[79-81] were observed from the CD spectra of L6 using BestSel analysis showing a dominant percentage of an α-helical structure, dependent on peptide concentration (with 55 – 90% helical structure as concentration increased from 1 μM to 1 mM) (Figure 3 and Table S2). While other methods such as SELCON,[82] CONTIN,[83] and CDSSTR[84] could be used to estimate the proportion of α-helical structures fairly accurately by using the data collected from the CD spectra,

the BeStSel method includes more specific β-sheet structures that otherwise could be mistaken for α-helical structures.[57] However, it should be noted that the BeStSel method, as with other mentioned methods, has basis spectra determined mostly on proteins with known secondary structures. Proteins generally do not contain high portions of aromatic residues in their structure. For example, when using the NCBI database,[85] the frequency of occurrence of aromatic residues in proteins, in general, was found to be very low compared to other natural amino acid residues (at 1.32% , 3.25%, and 3.91% for tryptophan, phenylalanine, and tyrosine respectively).[28] As the indole chromophore present in the aromatic residues could interfere with the CD spectra, [86, 87] this may affect the predicted secondary structure when using analysis tools such as BeStSel. Therefore, such CD spectra analysis tools should be used with caution. For further insights into the peptide secondary structure, all-atom MD simulation of one L6 peptide monomer was carried out. The FEL of L6 showed 3 energy minima (Figure S2), primarily α-helical, with two minima showing a representative peptide structure having distortions at the ends while maintaining an α-helical structure in the middle. The calculated RMSF for L6 highlights the flexibility of movement in residues 1 – 3, 13 – 16, and 19 – 21 (Figure S3). The flexibility at both ends of the L6 peptide chain could be associated with the lack of peptide-peptide interactions to stabilise the designed α-helical L6 structure. As per the CD spectroscopy results, by increasing the concentration the chances of inter-molecular stabilisation increase and therefore a higher α-helical content was observed.

To assess the effect of aromatic residues on the α-helical structure and self-assembly into fibrillar shapes, the F6 sequence was designed whereby all six Leu residues in L6 were replaced by Phe. The F6 thickened on titration with sodium bicarbonate to pH 7.4,[22] indicating self-assembly. Self-assembly of F6 into fibrils was also confirmed by AFM imaging[22], and the CG model also showed a fibrillar structure (Figure 1). The CD spectra of F6 showed the characteristic peaks of an α-helical structure, although being less distinct and intense when compared to L6 at all concentrations (Figure 3). By diluting the concentration from 1000 µM to 1 µM, the ellipticity at 222 nm for L6 and F6 dropped by about 40% and 70% (from -36,000 and -25,000 deg cm^2 dmol^{-1} at 1000 µM), respectively (Figure 3 and Table S2).

Using BeStSel, the percentage of α-helical structure for L6 and F6 at 1000 µM was calculated to be around 89% and 86%, respectively, while at 1 µM concentration, it was found to be 53% and 31%, respectively (Figure 3 and Table S2), indicating that incorporation of the Phe residue has resulted in a slight decrease in percentage of α-helical structure. This may be due to steric hindrance compared to the Leu residue and aromatic-aromatic interactions affecting the α-helical secondary structure stability.

W6 was tested to assess how increasing steric hindrance of the aromatic residues could affect the peptide structure. This W6 peptide was designed such that all six Leu residues at the *a* and *d* positions in L6 were replaced by Trp residues. The α-helical content of W6 at all concentrations, assessed using CD spectroscopy, was greatly reduced compared to both L6 and F6, as seen in Figure 3 and Table S2. Accordingly, substituting the aliphatic L with the aromatic residue W disrupts the α-helical structure. While the CD spectra of W6 are not characteristic of any secondary structure, BeStSel curve fitting suggests that a β-sheet may be the most prominent of the most common secondary structures (Figure 3). The bulky Trp residues may have reduced the range of sterically acceptable conformations for α-helices, and it seems more likely that the presence of

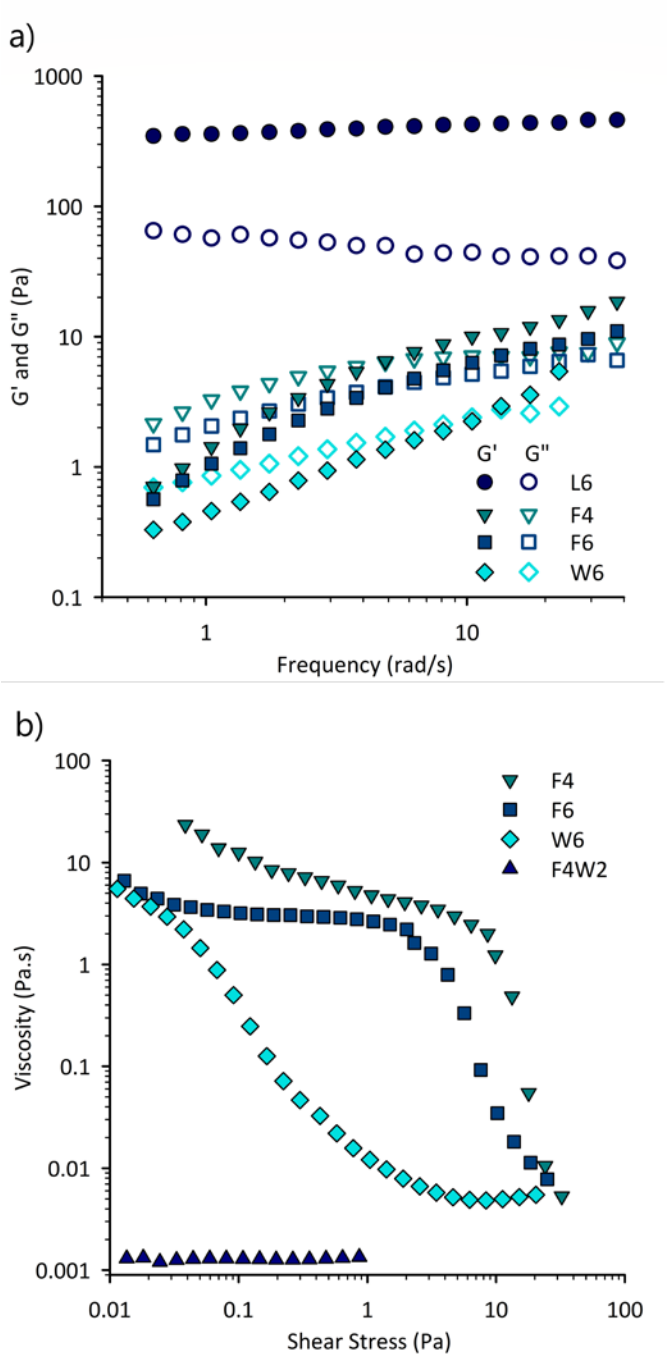

Figure 2. (a) Storage and Loss modulus as a function of frequency in the linear viscoelastic regime. G' filled and G" open symbols and (b) Viscosity as a function of shear stress showing a range of rheological behaviour for F4 and F6 (apparent yield stress fluids), W6 (highly shear thinning) and F4W2 (Newtonian) at a concentration of 5 mM, tested at least 1 hour after titration with sodium bicarbonate.

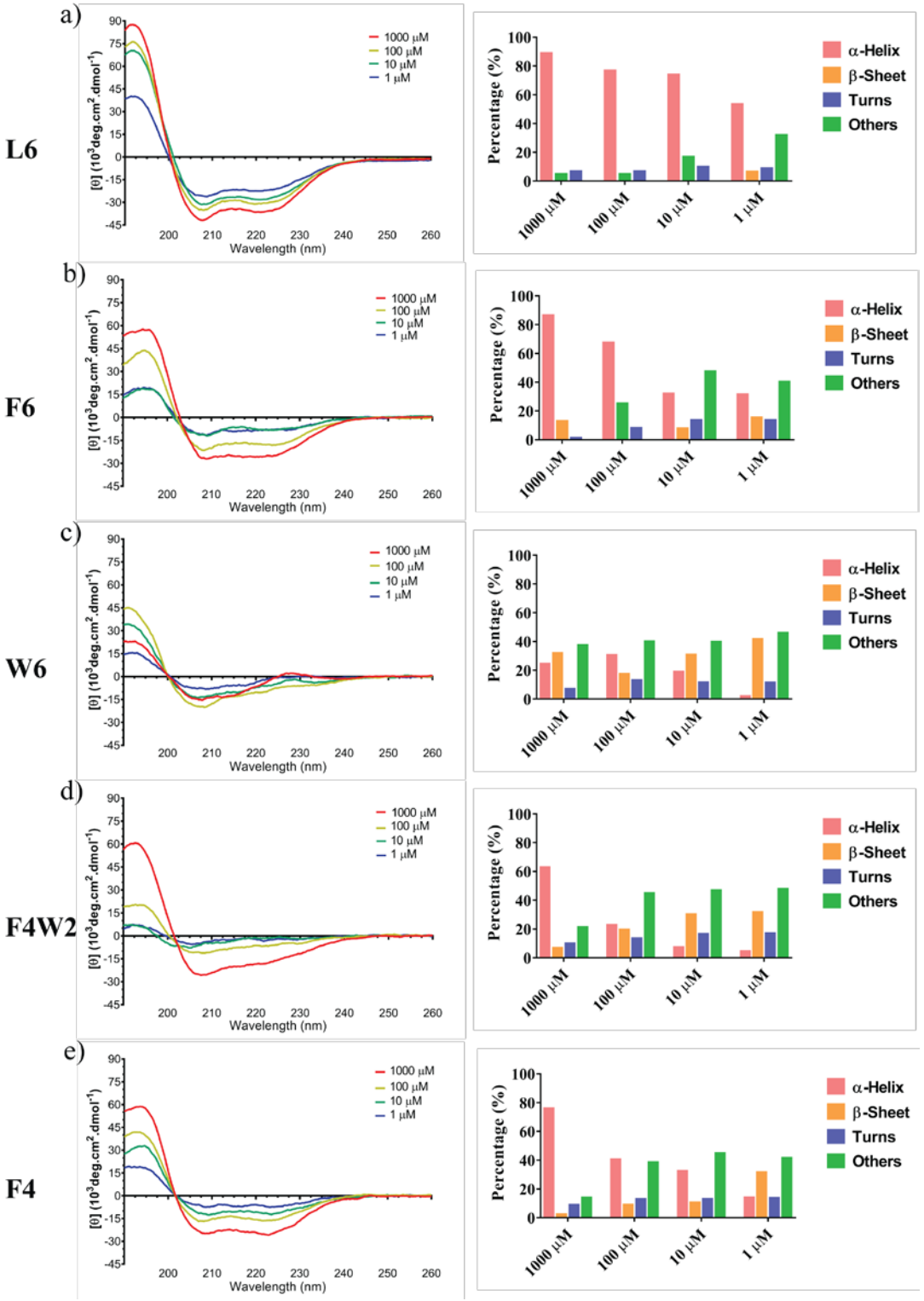

Figure 3. CD spectra on the left and secondary structure estimated by BeStSel[55] on the right for (a) L6, (b) F6, (c) W6, (d) F4W2, and (e) F4 peptides indicating the possible changes in secondary structure at 1 mM, 100 µM, 10 µM, and 1 µM concentrations.

hydrogen-bond acceptors on the Trp sidechain provided alternative mechanisms of stabilisation, favouring β-sheet structure formation.[88, 89] The average $MOI_{(z/x)}$ value for the CG model cluster of W6 was the lowest of all the peptides tested (Figure S4).The aggregated W6 was less one-dimensional (i.e., less fibrillar), showing a high dimension aggregated assembled shape (Figure S4 and Figure 1). The AFM images of W6 titrated with sodium bicarbonate revealed aggregate shapes with appendages similar to protofibrils, supported by the modelling showing a non-fibrillar shape (Figure 1). W6 was found to be a

viscoelastic fluid with G'<G" up to a frequency 10 rad/s (Figure 2). As shown in Figure 2b, W6 has a viscosity of the order of 10 Pa.s at a low shear rate with highly shear thinning behaviour. The rheology in combination with the AFM results suggests weak interactions between aggregates within the system that are able to break and align in the direction of flow during the application of shear.

The incorporation of six Trp residues into L6 (i.e., to form W6) completely disrupted the α-helical structure and coiled-coil formation (Figure 1 and Figure 3). Based on the CD spectra and molecular modelling of F6 and W6, Phe seems to have a reduced destabilising effect on the α-helical peptide structure and resulting self-assembly than Trp (Figure 1 and Figure 3). This, in turn, suggests an adverse effect due to steric hindrance and a destabilising effect via associated hydrogen-bonding interaction of the Trp indole side chain. Therefore, a combination of both aromatic residues was used in F4W2 to compare the effect of both on the α-helical structure and peptide self-assembly. Four out of six aromatic residues in the first two heptad repeats of W6 were replaced by Phe in the F4W2 peptide in order to assess how the incorporation of a less bulky aromatic residue with less ability to form hydrogen bonding could affect the peptide secondary structure and self-assembly. Unlike F6 and W6, F4W2 was not observed to thicken upon titration to pH 7.4. However, unlike W6, the CG model of F4W2 showed a fibrillar shape with branching, and the AFM image of the titrated F4W2 indicated fibril formation (Figure 1). G' and G" are very low, below the measurement range of the rheometer, supported by the Newtonian viscosity (Figure 2b). The measurement of Newtonian viscosity suggests that the fibrillar structures formed upon titration with sodium bicarbonate have a very small hydrodynamic volume and little or no interactions between them.

The ability of F4W2 to form fibrils should be associated with an increased α-helical content as the higher the α-helical content, the higher the chance of coiled-coil formation and fibril formation through a slippage mechanism. The α-helical content as estimated by BeStSel at the highest tested concentration (1 mM) for F4W2 was about 63%, which is higher than for W6 at the same concentration (at about 24% α-helical content, see Figure 3 and Table S2). This suggests that a higher α-helical content promoted assembly of F4W2 into fibrillar structures.

We hypothesise that the positioning of Trp residues close to the N-terminus could be the cause of disruption of the peptide self-assembly, based on the previous discussion around F4W2 assembly. Based on these results, a new peptide design W2F4 (Table 1) was modelled, with the Trp residues in the last two heptad repeats of W6 substituted by Phe residues. The CG model of W2F4 showed no characteristics of a fibril, as observed in F4W2, but rather a planar shape (Figure S5). These MD results support the importance of incorporating aromatic residues close to the N-terminus on the peptide self-assembly.

The incorporation of aromatic residues into the de-novo designed 21-mer peptide, L6, showed disruption to the α-helical structure of that peptide and affected the self-assembly. This was not unexpected, as the disruptive effect of aromatic residue incorporation on peptide a-helical stability has been reported.[43, 90] This suggests that the incorporation of fewer aromatic residues should reduce the disruption of the α-helical structure. Therefore, it was decided to decrease the number of Phe residues in F6 from six to four. While the incorporation of aromatic residues was carried out at the conventional *a* and *d* positions in the hydrophobic core, it was decided to assess the effect of the aromatic residue position in the peptide sequence. Three of the Phe residues in the F4 design replaced the Leu residues at the *d* position in L6 while the fourth Phe residue in F4 replaced a Leu residue at the *g* position in the second heptad repeat. While the *e* and *g* positions were designed in L6 to extend the hydrophobic core, these positions are more exposed to the aqueous environment compared to *a* and *d* positions. Therefore, the presence of a Phe residue at the *g* position in F4 could cause disruption to the α-helical structure. However, having an aromatic residue at the *g* position could raise the possibility of aromatic-aromatic interactions with aromatic residues of other peptide monomers, which is beneficial to explore (considering the possible addition of different pathways for electron transfer through aromatic-aromatic interactions). The possibility of aromatic residues interacting with other aromatic residues of a different peptide monomer could be affected by peptide concentration and therefore affect the peptide assembly and peptide α-helical structure in a more complex way.

F4 was observed to thicken upon titration with sodium bicarbonate. Both F4 and F6 were observed to be viscoelastic fluids with G' < G" up to a frequency of 5 rad/s (Figure 2a). As shown in Figure 2b, samples F4 and F6 have a viscosity of the order of 10 Pa.s at a low shear rate with apparent yield stress behaviour for F4 and F6 at 9 Pa and 2 Pa, respectively. Note, rheology alone cannot be used to elucidate the structure of a material, and complementary techniques such as AFM should be used. This is especially true for the small differences in rheology observed here between F4 and F6. The CG model of F4 and its AFM image both showed a fibrillar structure (Figure 1) with an average $MOI_{(z/x)}$ of 5.27 (Table S1). Regarding the peptide self-assembly, since they were designed to self-assemble into fibrils by a "slippage" model,[11] the greater flexibility of the third heptad may be crucial for the alignment of bulky aromatic residues in the hydrophobic core and continuation of the assembled structures. On the other hand, in all heptad repeats in F4, Leu and Phe were located at the *a* and *d* positions, respectively, increasing the chance of forming a Phe-Leu zipper assembly. F6 showed a greater fluctuation at the peptide chain ends compared to F4 (Figure S3), and the fibril structure observed by CG modelling was more branched (Figure 1). The CD spectra of F4 were characteristic of α-helices, although of lower intensity and slightly red-shifted compared to L6 (Figure 3). The α-helical content as calculated by BeStSel analysis was 76%, 40%, 32%, and 14% for 1 mM, 100 μM, 10 μM, and 1 μM F4, respectively (Figure 3 and Table S2). This is lower than α-helical content of L6 but higher than F4W2 and W6. The peptide containing the highest Phe content, F6, was found to have a slightly higher α- helical content than F4 (Figure 3 and Table S2). The placement of a Phe residue in the *g* position of the second heptad repeat (instead of in the conventional *a* and

d positions) in F4 may contribute to an altered self-assembly. Phe was placed at the *g* position in F4 in order to increase the interaction with aromatic residues from other peptides at the expense of being exposed to the aqueous environment, potentially destabilising the α-helical structure. At higher concentrations, both F6 and F4 maintained a primarily α-helical structure (Figure 3 (b) and (e)) and formed fibrillar structures (Figure 1 (d) and (e)), suggesting that intermolecular stabilisation by hydrophobic interactions may overcome any potential intramolecular steric hindrance caused by Phe.

At the lowest tested concentration (1 μM), F4 was estimated to have less than half the content of the α-helical structure compared to F6 (Figure 3 (b) and (e)). At lower concentrations, interactions between peptide monomers are at their lowest and, therefore, the Phe residue at the *g* position in F4 is more exposed to the aqueous environment and less able to interact with Phe residues of other peptide monomers. This could lead to destabilising of the peptide α-helical structure as Phe residues between different peptide monomer stabilise through aromatic-aromatic interactions. The FEL created from the all-atom MD of one peptide monomer shows two stable representative structures of F4 (Figure S2). In one of these representative structures, the α-helical structure is disrupted in the middle of the chain (where the Phe residue at the *g* position is located). At low concentrations, the Phe residue at this position may be stabilised by intramolecular interactions, potentially disrupting the peptide α-helical structure (Figure S2). This observation may explain why F4 was able to form a fibrillar structure at higher concentrations but showed a much lower α-helical content at lower concentrations compared to F6.

Conclusion

In our designs, F6 showed to retain its α-structure relatively better than F4 while diluted suggesting the importance of aromatic residue positioning. The importance of aromatic residue position on peptide structure should not be overseen, although to fully understand and compare its significance versus density of aromatic residues further peptide designs should be tested. F6 retained its α-structure relatively better than F4 while diluted suggesting some importance of aromatic residue positioning with regards to the hydrophobic core. These results suggest that aromatic residues ought to be restrained to the core positioning (*a* and *d* positions), as has been utilised in previous studies.[32, 87, 91] When using only the conventional *a* and *d* positions for placement of the aromatic residues, the incorporation of aromatic residues in the first heptad had an adverse effect on peptide self-assembly compared to when these residues were placed in the third heptad, close to the C-terminus. While the importance of parameters such as hydrophobicity, steric effects, and helical forming propensity is outlined in the literature for designing a stable α-helical structure, the chemistry of side chains is crucial when considering aromatic residues due to their adjacent steric hindrance and hydrogen-bonding. Our study suggests that Trp residues should be used sparingly in the design α-helical peptides, while a higher tolerance may be observed for Phe residues. For further insights, future studies on additional aromatic-containing peptide designs may build on this work to assess the effect of aromatic residues on the peptide α-helical structure and fibril formation.

Conflicts of interest

The authors declare that they have no conflicts of interest with the contents of this article.

Acknowledgements

Financial support was provided by the Australian Research Council (Grant ID DP150100268 and DP140103653) and the Australian Government Research Training Program (RTP) Scholarship. T.A.H.N and A.S acknowledge the University of Queensland's Research Computing Centre (RCC) for its support in this research. This work was performed in part at the Queensland node of the Australian National Fabrication Facility, a company established under the National Collaborative Research Infrastructure Strategy to provide nano- and micro-fabrication facilities for Australia's researchers. The authors would like to thank Professor Jason Stokes for the use of the rheology laboratory. H.M.S acknowledges salary funding from the Australian Research Council LP160100239. The authors also would like to thank Professor Vincent Conticello for the use of TEM imaging facility in Emory University and acknowledge the associated funding from National Science Foundation, Division of Materials Research (NSF DMR 1533958). The authors would like to thank Dr. Andrea Merg and Ms. Ordy Gnewou for helpful advice on acquiring TEM images.

References

1. L. Bragg, J. C. Kendrew and M. F. Perutz, *Proceedings of the Royal Society of London A*, 1950, **203**, 321-357.
2. Z. Shi, C. A. Olson, A. J. Bell and N. R. Kallenbach, *Peptide Science*, 2001, **60**, 366-380.
3. R. S. Hodges, *Biochemistry and cell biology*, 1996, **74**, 133-154.
4. A. Lupas, *Trends in biochemical sciences*, 1996, **21**, 375-382.
5. E. H. Bromley, K. Channon, E. Moutevelis and D. N. Woolfson, *ACS chemical biology*, 2008, **3**, 38-50.
6. A. D. McLachlan and M. Stewart, *J Mol Biol*, 1975, **98**, 293-304.
7. D. A. Parry, *Bioscience reports*, 1982, **2**, 1017-1024.
8. C. N. Pace and J. M. Scholtz, *Biophysical journal*, 1998, **75**, 422-427.
9. A. Yakimov, A. Afanaseva, M. Khodorkovskiy and M. Petukhov, *Acta Naturae (англоязычная версия)*, 2016, **8**.
10. K. T. O'Neil and W. F. DeGrado, *Science*, 1990, **250**, 646-651.
11. N. L. Fletcher, C. V. Lockett and A. F. Dexter, *Soft Matter*, 2011, **7**, 10210-10218.
12. J. Liu, Q. Zheng, Y. Deng, N. R. Kallenbach and M. Lu, *Journal of molecular biology*, 2006, **361**, 168-179.

13. J. Cory-Wright, M. Alqazzaz, F. Wroe, J. Jeffreys, L. Zhou and S. C. Lummis, *ACS chemical neuroscience*, 2017, **9**, 284-290.
14. R. K. Spencer and A. I. Hochbaum, *Biochemistry*, 2017, **56**, 5300-5308.
15. N. S. Malvankar and D. R. Lovley, *Current Opinion in Biotechnology*, 2014, **27**, 88-95.
16. K. A. McAllister, H. Zou, F. V. Cochran, G. M. Bender, A. Senes, H. C. Fry, V. Nanda, P. A. Keenan, J. D. Lear and J. G. Saven, *Journal of the American Chemical Society*, 2008, **130**, 11921-11927.
17. V. Zorbas, A. L. Smith, H. Xie, A. Ortiz-Acevedo, A. B. Dalton, G. R. Dieckmann, R. K. Draper, R. H. Baughman and I. H. Musselman, *Journal of the American Chemical Society*, 2005, **127**, 12323-12328.
18. F. A. Mann, J. Horlebein, N. F. Meyer, D. Meyer, F. Thomas and S. Kruss, *Chemistry–A European Journal*, 2018.
19. S. Li, A. N. Aphale, I. G. Macwan, P. K. Patra, W. G. Gonzalez, J. Miksovska and R. M. Leblanc, *ACS applied materials & interfaces*, 2012, **4**, 7069-7075.
20. R. C. Creasey, A. B. Mostert, T. Nguyen, B. Virdis, S. Freguia and B. Laycock, *Acta biomaterialia*, 2018.
21. N. L. Ing, M. Y. El-Naggar and A. I. Hochbaum, *The Journal of Physical Chemistry B*, 2018, **122**, 10403-10423.
22. R. C. G. Creasey, B. Mostert, A. Solemanifar, T. Nguyen, B. Virdis, S. Freguia and B. Laycock, *ACS Omega*, 2019.
23. M. Reches and E. Gazit, *Science*, 2003, **300**, 625-627.
24. E. Gazit, *Chemical Society Reviews*, 2007, **36**, 1263-1269.
25. T. M. Doran, A. J. Kamens, N. K. Byrnes and B. L. Nilsson, *Proteins: Structure, Function, and Bioinformatics*, 2012, **80**, 1053-1065.
26. C. J. Bowerman and B. L. Nilsson, *Peptide Science*, 2012, **98**, 169-184.
27. R. Orbach, I. Mironi-Harpaz, L. Adler-Abramovich, E. Mossou, E. P. Mitchell, V. T. Forsyth, E. Gazit and D. Seliktar, *Langmuir*, 2012, **28**, 2015-2022.
28. E. Gazit, *The FASEB Journal*, 2002, **16**, 77-83.
29. M. Reches and E. Gazit, *Current Nanoscience*, 2006, **2**, 105-111.
30. E. Gazit, *The FEBS journal*, 2005, **272**, 5971-5978.
31. R. B. Hill and W. F. DeGrado, *Journal of the American Chemical Society*, 1998, **120**, 1138-1145.
32. S. M. Butterfield, P. R. Patel and M. L. Waters, *Journal of the American Chemical Society*, 2002, **124**, 9751-9755.
33. R. Mahalakshmi, A. Sengupta, S. Raghothama, N. Shamala and P. Balaram, *The Journal of peptide research*, 2005, **66**, 277-296.
34. R. Bhattacharyya, U. Samanta and P. Chakrabarti, *Protein engineering*, 2002, **15**, 91-100.
35. M. M. Slutsky and E. N. G. Marsh, *Protein science*, 2004, **13**, 2244-2251.
36. O. D. Monera, T. J. Sereda, N. E. Zhou, C. M. Kay and R. S. Hodges, *Journal of peptide science: an official publication of the European Peptide Society*, 1995, **1**, 319-329.
37. C. Guo, X. Yu, S. Refaely-Abramson, L. Sepunaru, T. Bendikov, I. Pecht, L. Kronik, A. Vilan, M. Sheves and D. Cahen, *Proceedings of the National Academy of Sciences*, 2016, **113**, 10785-10790.
38. N. Amdursky, *Physical Chemistry Chemical Physics*, 2013, **15**, 13479-13482.
39. N. L. Ing, R. K. Spencer, S. H. Luong, H. D. Nguyen and A. I. Hochbaum, *ACS Nano*, 2018, **12**, 2652-2661.
40. F. H. Crick, *Acta crystallographica*, 1953, **6**, 689-697.
41. B. Apostolovic and H.-A. Klok, *Biomacromolecules*, 2008, **9**, 3173-3180.
42. B. Apostolovic, M. Danial and H.-A. Klok, *Chemical Society Reviews*, 2010, **39**, 3541-3575.
43. C. T. Armstrong, A. L. Boyle, E. H. Bromley, Z. N. Mahmoud, L. Smith, A. R. Thomson and D. N. Woolfson, *Faraday discussions*, 2009, **143**, 305-317.
44. Y. Deng, J. Liu, Q. Zheng, D. Eliezer, N. R. Kallenbach and M. Lu, *Structure*, 2006, **14**, 247-255.
45. J. Liu, Q. Zheng, Y. Deng, C.-S. Cheng, N. R. Kallenbach and M. Lu, *Proceedings of the National Academy of Sciences*, 2006, **103**, 15457-15462.
46. N. R. Zaccai, B. Chi, A. R. Thomson, A. L. Boyle, G. J. Bartlett, M. Bruning, N. Linden, R. B. Sessions, P. J. Booth and R. L. Brady, *Nature chemical biology*, 2011, **7**, 935.
47. J. R. Litowski and R. S. Hodges, *Journal of Biological Chemistry*, 2002, **277**, 37272-37279.
48. N. E. Zhou, C. M. Kay and R. Hodges, *Journal of Biological Chemistry*, 1992, **267**, 2664-2670.
49. E. F. Banwell, E. S. Abelardo, D. J. Adams, M. A. Birchall, A. Corrigan, A. M. Donald, M. Kirkland, L. C. Serpell, M. F. Butler and D. N. Woolfson, *Nature materials*, 2009, **8**, 596.
50. E. H. Bromley, K. J. Channon, P. J. King, Z. N. Mahmoud, E. F. Banwell, M. F. Butler, M. P. Crump, T. R. Dafforn, M. R. Hicks and J. D. Hirst, *Biophysical journal*, 2010, **98**, 1668-1676.
51. M. J. Pandya, G. M. Spooner, M. Sunde, J. R. Thorpe, A. Rodger and D. N. Woolfson, *Biochemistry*, 2000, **39**, 8728-8734.
52. M. G. Ryadnov and D. N. Woolfson, *Angewandte Chemie International Edition*, 2003, **42**, 3021-3023.
53. H. Dong, S. E. Paramonov and J. D. Hartgerink, *Journal of the American Chemical Society*, 2008, **130**, 13691-13695.
54. K. Pagel, S. C. Wagner, K. Samedov, H. von Berlepsch, C. Böttcher and B. Koksch, *Journal of the American Chemical Society*, 2006, **128**, 2196-2197.
55. S. a. Potekhin, T. Melnik, V. Popov, N. Lanina, A. a. Vazina, P. Rigler, A. Verdini, G. Corradin and A. Kajava, *Chemistry & biology*, 2001, **8**, 1025-1032.
56. A. Dexter, N. Fletcher, R. Creasey, F. Filardo, M. Boehm and K. Jack, *RSC Advances*, 2017, **7**, 27260-27271.
57. A. Micsonai, F. Wien, L. Kernya, Y. H. Lee, Y. Goto, M. Refregiers and J. Kardos, *Proc Natl Acad Sci U S A*, 2015, **112**, E3095-3103.
58. A. Micsonai, F. Wien, E. Bulyaki, J. Kun, E. Moussong, Y. H. Lee, Y. Goto, M. Refregiers and J. Kardos, *Nucleic Acids Res*, 2018, **46**, W315-W322.
59. S. J. Marrink, H. J. Risselada, S. Yefimov, D. P. Tieleman and A. H. De Vries, *The journal of physical chemistry B*, 2007, **111**, 7812-7824.
60. L. Monticelli, S. K. Kandasamy, X. Periole, R. G. Larson, D. P. Tieleman and S.-J. Marrink, *Journal of chemical theory and computation*, 2008, **4**, 819-834.
61. D. H. de Jong, G. Singh, W. D. Bennett, C. Arnarez, T. A. Wassenaar, L. V. Schäfer, X. Periole, D. P. Tieleman and S. J. Marrink, *Journal of Chemical Theory and Computation*, 2012, **9**, 687-697.
62. S. J. Marrink, H. J. Risselada, S. Yefimov, D. P. Tieleman and A. H. de Vries, *The Journal of Physical Chemistry B*, 2007, **111**, 7812-7824.
63. Schrodinger, LLC, *Journal*, 2015.

64. M. J. Abraham, T. Murtola, R. Schulz, S. Páll, J. C. Smith, B. Hess and E. Lindahl, *SoftwareX*, 2015, **1**, 19-25.
65. R. B. Best, X. Zhu, J. Shim, P. E. Lopes, J. Mittal, M. Feig and A. D. MacKerell Jr, *Journal of chemical theory and computation*, 2012, **8**, 3257-3273.
66. P. Mark and L. Nilsson, *The Journal of Physical Chemistry A*, 2001, **105**, 9954-9960.
67. B. Hess, H. Bekker, H. J. Berendsen and J. G. Fraaije, *Journal of computational chemistry*, 1997, **18**, 1463-1472.
68. T. Darden, D. York and L. Pedersen, *The Journal of chemical physics*, 1993, **98**, 10089-10092.
69. F. Sohraby, M. Bagheri and H. Aryapour, in *Computational Methods for Drug Repurposing*, Springer, 2019, pp. 23-43.
70. I. Wolfram Research, *Mathematica*, Wolfram Research, Inc., Champaign, Illinois, Version 10.0 edn., 2014.
71. W. Humphrey, A. Dalke and K. Schulten, *Journal of molecular graphics*, 1996, **14**, 33-38.
72. S. J. Marrink, A. H. De Vries and A. E. Mark, *The Journal of Physical Chemistry B*, 2004, **108**, 750-760.
73. S. Yesylevskyy and C. Ramseyer, *Physical Chemistry Chemical Physics*, 2014, **16**, 17052-17061.
74. A. Micsonai, BeStSel, http://bestsel.elte.hu, (accessed March, 2019).
75. G. A. Davies and J. R. Stokes, *Journal of Rheology*, 2005, **49**, 919-922.
76. G. Davies and J. Stokes, *Journal of Non-newtonian fluid mechanics*, 2008, **148**, 73-87.
77. O. Kravchuk and J. R. Stokes, *Journal of Rheology*, 2013, **57**, 365-375.
78. A. V. Martinez, L. Dominguez, E. Małolepsza, A. Moser, Z. Ziegler and J. E. Straub, *The Journal of Physical Chemistry B*, 2013, **117**, 7345-7351.
79. N. J. Greenfield, *Nature protocols*, 2006, **1**, 2876-2890.
80. A. J. Adler, N. J. Greenfield and G. D. Fasman, in *Methods in enzymology*, Elsevier, 1973, vol. 27, pp. 675-735.
81. Y.-H. Chen, J. T. Yang and K. H. Chau, *Biochemistry*, 1974, **13**, 3350-3359.
82. N. Sreerama, S. Y. Venyaminov and R. W. Woody, *Protein Science*, 1999, **8**, 370-380.
83. S. W. Provencher and J. Gloeckner, *Biochemistry*, 1981, **20**, 33-37.
84. N. Sreerama and R. W. Woody, *Analytical biochemistry*, 2000, **287**, 252-260.
85. R. C. Beavis and D. Fenyö, Amino Acids, http://prowl.rockefeller.edu/aainfo/struct.htm, (accessed March 05, 2019).
86. H.-E. Lee, J. Lee, M. Ju, H.-Y. Ahn, Y. Y. Lee, H.-S. Jang and K. T. Nam, *Molecular Systems Design & Engineering*, 2018, **3**, 581-590.
87. J. Liu, W. Yong, Y. Deng, N. R. Kallenbach and M. Lu, *Proceedings of the National Academy of Sciences*, 2004, **101**, 16156-16161.
88. S. V. R. Jonnalagadda, E. Ornithopoulou, A. A. Orr, E. Mossou, V. T. Forsyth, E. P. Mitchell, M. W. Bowler, A. Mitraki and P. Tamamis, *Molecular Systems Design & Engineering*, 2017, **2**, 321-335.
89. K. Fujiwara, H. Toda and M. Ikeguchi, *BMC structural biology*, 2012, **12**, 18.
90. A. L. Boyle and D. N. Woolfson, *Chemical Society Reviews*, 2011, **40**, 4295-4306.
91. S. Aravinda, N. Shamala, C. Das, A. Sriranjini, I. L. Karle and P. Balaram, *Journal of the American Chemical Society*, 2003, **125**, 5308-5315.